

Article

Assimilating Aeolus Satellite Wind Data on a Regional Level: Application in a Mediterranean Cyclone Using the WRF Model

Christos Stathopoulos^{1,2,*}, Ioannis Chaniotis^{1,2} and Platon Patlakas^{1,2,*} 

¹ Department of Physics, National and Kapodistrian University of Athens, 15784 Athens, Greece; giannisch@mg.uoa.gr

² Weather and Marine Engineering Technologies P.C., 17456 Alimos, Greece

* Correspondence: chrisstath@mg.uoa.gr (C.S.); platon@mg.uoa.gr (P.P.)

Abstract: This study uses a limited area model to improve the understanding of assimilating Aeolus Level 2B wind profiles on a regional level under severe weather conditions. Aeolus wind profile measurements have offered new insights into weather analysis and applications. The assimilation of Aeolus Level 2B winds has enhanced the observed state of the atmosphere spatially and temporally in global modeling systems. This work is focused on the development and evolution of a Mediterranean tropical-like cyclone that occurred between 27–30 September 2018. Aeolus coverage had a good spatial and temporal alignment with the broader area and time periods during which the cyclone originated and developed, affording the opportunity to explore the direct influence of Aeolus satellite retrievals in model initialization processes. Using the WRF 3DVar modeling system, model results showcase the effects stemming from Aeolus data ingestion, with the main differences presenting after the first 24 h of simulation. Smaller or larger deviations in the runs with and without the Aeolus wind data assimilation are evident in most cyclonic characteristics, extending vertically up to the mid-troposphere. The absence of a consistent trend in cyclone intensification or weakening underlines the unique impact of the Aeolus dataset in each case.

Keywords: data assimilation; numerical weather prediction; Aeolus satellite data; Mediterranean cyclones



Citation: Stathopoulos, C.; Chaniotis, I.; Patlakas, P. Assimilating Aeolus Satellite Wind Data on a Regional Level: Application in a Mediterranean Cyclone Using the WRF Model. *Atmosphere* **2023**, *14*, 1811. <https://doi.org/10.3390/atmos14121811>

Academic Editors: Rosa Claudia Torcasio, Stefano Federico and Elenio Avolio

Received: 10 November 2023

Revised: 3 December 2023

Accepted: 6 December 2023

Published: 11 December 2023



Copyright: © 2023 by the authors. Licensee MDPI, Basel, Switzerland. This article is an open access article distributed under the terms and conditions of the Creative Commons Attribution (CC BY) license (<https://creativecommons.org/licenses/by/4.0/>).

1. Introduction

The Mediterranean Sea is characterized by intense cyclonic activity. A wide range of atmospheric processes associated with large-scale circulation and combined with the complex topographical features, including the intense land–sea contrasts, favor cyclogenesis in the region [1]. Commonly, the generated cyclones in the semi-closed Mediterranean basin exhibit weak characteristics in terms of lifetime, structure, size and intensity compared to the tropical and mid-latitude cyclones formed in open seas. On a not particularly rare basis, however, Mediterranean cyclones could transit into tropical-like cyclones (TLCs), sharing many features with their tropical counterparts [2]. These severe weather events, also referred to as medicanes, have received a lot of attention from the research community [3–5], due to their complexity and destructive effects, specifically when reaching coastal zones.

Relevant studies on Mediterranean cyclones involve the use of Numerical Weather Prediction (NWP) models and the utilization of both conventional and advanced observations [6–8]. The latest and ongoing advances in NWP models have offered many improvements in the understanding and description of complex and rapidly developed weather phenomena. An important aspect in the efficiency of NWP simulations, is the sufficiency and reliability of the initial and boundary data used [9,10]. Data assimilation is a technique for improving the description of the initial state of both the atmosphere and surface with the ingestion of observation data into the model grid [11]. A drawback in the various data assimilation approaches is the lack of quality or complete absence of observations for ingestion. Moreover, in many regions, the existing surface, upper air and remote sensing data are often sparse both in the horizontal and vertical scale.

In this context, ongoing efforts have been made to counterbalance the aforementioned deficiencies in the availability of observational data with the release of new products. One important aspect is the measurements for direct wind profiles that have proved to offer positive feedback in a number of studies and services [12–14]. In most cases, the observed state of the atmosphere related to the wind profile is partially covered by radiosondes, aircraft and satellites, with many listed limitations in frequency and spatial availability. Aiming to address this deficiency, the European Space Agency (ESA) launched the Aeolus satellite, a polar-orbiting wind profiler, providing vertical wind speed distribution detected by an onboard Doppler wind lidar system [15]. This is the first satellite-based Doppler wind lidar mission, intended to enable regional and global NWP systems to incorporate accurate wind shear information, vital for diagnosing turbulence and predicting the development of baroclinic weather systems with the use of high-resolution wind data with precise height assignment [16]. Many studies have focused on the evaluation and quality assessment of Aeolus wind profile measurements [17], using equivalent radiosonde, model and other types of satellite-derived wind information, highlighting some of the scientific benefits of the Aeolus Doppler Wind Lidar mission. Notable improvements have also been shown in forecasts with the ingestion of Aeolus winds in global forecasting systems, and plenty of operational centers have adopted this wind product in their data assimilation techniques [18–21]. Likewise, but to a lesser extent, the benefits from Aeolus data implementation have been demonstrated in experimental studies carried out with limited area models (LAMs) [22–25].

In this work, the impact of assimilating Aeolus wind profile winds is assessed, focusing on the development and evolution of a Mediterranean cyclone. More precisely, the main objective is to further investigate the effects and potential benefits in the initial conditions and, subsequently, the cyclone predictability from assimilating wind profiles at a regional level. For the needs of the study, numerical experiments focused on medicane Zorbas, which occurred in September 2018, were conducted. The medicane developed in the Ionian Sea, an active zone of cyclogenesis, and is a characteristic recent case of a destructive cyclone that led to excessive wind speeds and severe rainfalls inland.

The structure of the paper is organized as follows: Section 1 describes the modeling system used. The methodology, input data and the experimental case are presented in Section 2. Analysis, results of the performed experiments and evaluation are discussed in Section 3. Further discussion and conclusions are presented in Section 4.

2. Materials and Methods

2.1. WRF Model

The atmospheric model used for the numerical experiments of this study is the Advanced Research (ARW) WRF version 3.9.1 [26]. It is a non-hydrostatic, atmospheric model which has been extensively used both for research and operational purposes (e.g., [27]). The WRF model provides a suite of advanced dynamics, physics and numerical schemes for simulating a wide range of meteorological processes. One of its strengths lies in its ability to offer data assimilation schemes that can effectively incorporate diverse observational inputs [28,29].

2.2. WRF Data Assimilation (DA)

The 3DVar (Three-Dimensional Variational) data assimilation technique in WRF combines NWP output, which is considered a first guess (or background field), observational data and the derived error statistics. In particular, an improved estimate is acquired by the minimization of a cost function:

$$J(x) = \frac{1}{2}(x - x^b)^T B^{-1}(x - x^b) + \frac{1}{2}(y - y^0)^T R^{-1}(y - y^0) \quad (1)$$

with x being the analysis field vector, x^b the background state vector, y the observation vector, B the background error covariance matrix, and R the observation error covariance

matrix. The y^0 is the ingested observation, while the $y = H(x)$ is the resultant model observation obtained from the analysis x through the observation operator H and fitted into the observation space. The goal is a solution for the minimization of the cost function $J(x)$ that represents an estimate of the true state of the atmosphere with minimum variance considering the first guess x^b and the assimilated observation y^0 .

2.3. Aeolus

The Aeolus satellite mission has the objective of retrieving high-quality wind profile datasets measured from the surface up to the lower stratosphere. A Doppler wind lidar instrument provides wind measurements in a near-Sun-synchronous, ~320 km altitude, dawn–dusk orbit [30]. The laser scans the atmosphere and the light is backscattered and analyzed to derive the Horizontal Line-of-Sight (HLOS) wind component profile that is a result of the measured wind along the laser beam line of sight. The analysis is based on two detection channels related to the diameters of the atmospheric particulates. The Rayleigh channel, that corresponds to molecular scattering and the Mie channel that detects the scattering from different types of aerosols and hydrometeors. From the various processed measurements, the L2B (Level 2B) products are oriented for data assimilation purposes [31]. The L2B wind profiles are separated into four observation categories; the Rayleigh-clear and Rayleigh-cloudy, covering a horizontal ground track close to 90 km, and the Mie-clear and Mie-cloudy, with a horizontal length of around 10 km. L2B winds are corrected for temperature and pressure broadening effects. Moreover, for data assimilation purposes, supplementary information is provided related to the quality of the records and the instrumental errors. Since 2020, the European Center for Medium-range Weather Forecasts (ECMWF) has started assimilating the Aeolus L2B products, particularly the Rayleigh-clear and Mie-cloudy types, noticing an overall improvement in the forecasting skill of the global forecasting system, the Integrated Forecasting System (IFS) [20].

2.4. Case Study

The study focuses on a Mediterranean cyclone, known as medicane Zorbas, that originated in the eastern Mediterranean waters. This cyclonic event impacted Greece heavily, mainly through hazardous high winds and heavy rainfall resulting in flooding. A detailed description of its origins and growth has been analyzed in [32], while the uncertainty enclosed in the triggering mechanisms has attracted the attention of several research studies [33,34]. The cyclone was formed over warm waters on 27 September 2018 and, starting from a spiral-like structure, quickly intensified, moving northeastward on the following day. Between the 28th and 29th, the cyclone had clearly acquired tropical-like characteristics with the formation of a cloud-free central eye. The tropical characteristics remained as it approached the southwest coastal zone of Greece. Having reached its peak on the 29th, the cyclone kept moving east-northeast on the following days and crossed the Aegean Sea where, through the interaction with land and the cooler waters, it dissipated.

2.5. Methodology

To investigate the effects of assimilating the Aeolus wind speed profiles, a number of experiments were performed, starting at times that coincided with the retrieval of L2B data. The model setup consists of two nests, an outer grid with a resolution of 12 km × 12 km and an inner grid of 4 km × 4 km, respectively. The first grid includes the whole Mediterranean Sea, while the fine one covers most of the eastern part of the basin with a spatial extension that encloses the track and magnitude of the cyclone under investigation. Further information about the model configuration is provided in Table 1.

Table 1. Configuration of the modeling system.

WRF V3.9.1 Atmospheric Model	
Model grids	Grid1: 12 km × 12 km, Grid2: 4 km × 4 km, two-way interactive nests
Input data	GFS analysis (00) and forecast (every 6 h) for initial and lateral boundary conditions (0.25° × 0.25° resolution), NCEP sea surface temperature daily analysis (5 arc-minutes)
Microphysics	Tompson scheme
Surface layer	Monin–Obukhov scheme [35]
Land–surface layer	Noah land–surface model [36]
Boundary layer	YSU scheme [37]
Turbulence Closure	Mellor–Yamada scheme 2.5
Radiation parameterization	Rapid Radiative Transfer Model (RRTM) [38]
Convective parameterization	Kain–Fritsch cumulus parameterization [39], none in inner grid

With the intention to examine the impact and the possible benefits of Aeolus winds in the description of medicane Zorbas, three types of simulation were performed in a cycling mode, using WRF model and its data assimilation module. It is worth mentioning that all experiments implemented the GFS data as an input for initial and lateral boundary conditions with the aim of inspecting the feedback of the proposed methods in forecasting mode. The first type of simulations included the control experiments without any data assimilation method in WRF. The second employed the WRF 3DVar system with the ingestion of conventional data for the improvement of initial and boundary conditions. Conventional data refer to ground observations, radiosondes, buoys and satellite-derived winds (Figure 1a). The third category of experiments included signals from both conventional observations and the Aeolus winds in the assimilation system. In both assimilation approaches, the NCM method [40] was used to calculate the background error, considering the differences between 12 h and 24 h forecasts valid at the same times of 15 days ahead. Despite the limited frequency of satellite coverage over specific regions, the Aeolus coverage had a good spatial and temporal alignment with the current event under investigation. This alignment closely corresponded to the broader area and time periods during which the cyclone, known as medicane Zorbas, originated and developed (Figure 1b). This circumstance presented an exceptional chance to explore the direct influence of Aeolus wind profiles during the initialization processes of the atmospheric model. Model initialization times together with the types of simulations are listed in Table 2.

For the implementation of the Aeolus Lev2B product, a number of quality control processes and criteria were applied before ingesting the data in the assimilation sub-model. Aeolus is a novel detection system with a continuous evolution and development of data availability, instrument performance and processing methods. Therefore, the criteria for quality correction are constantly reassessed and updated. In the current work, the Aeolus Lev2B winds (processor baseline 14) are post-processed based on a number of basic concepts for the elimination of invalid data (e.g., [22]). Primarily, wind data flagged as invalid were removed. HLOS winds only from Rayleigh-clear and Mie-cloudy types were used, considered as the ones with the better quality, in accordance with the ECMWF assimilation process [20]. Likewise, only data from altitudes above 250 m were selected. Moreover, data with instrumental errors above 6 m/s for Mie winds and 8 m/s for Rayleigh winds were also excluded. Figure 2 shows the distribution of Rayleigh-clear and Mie-cloudy HLOS winds before and after the implementation of the instrumental error-based correction, together with the vertical mean values and their deviation and the corresponding errors after the correction. The large deviations are attributed to the existence of both westerly and easterly wind components.

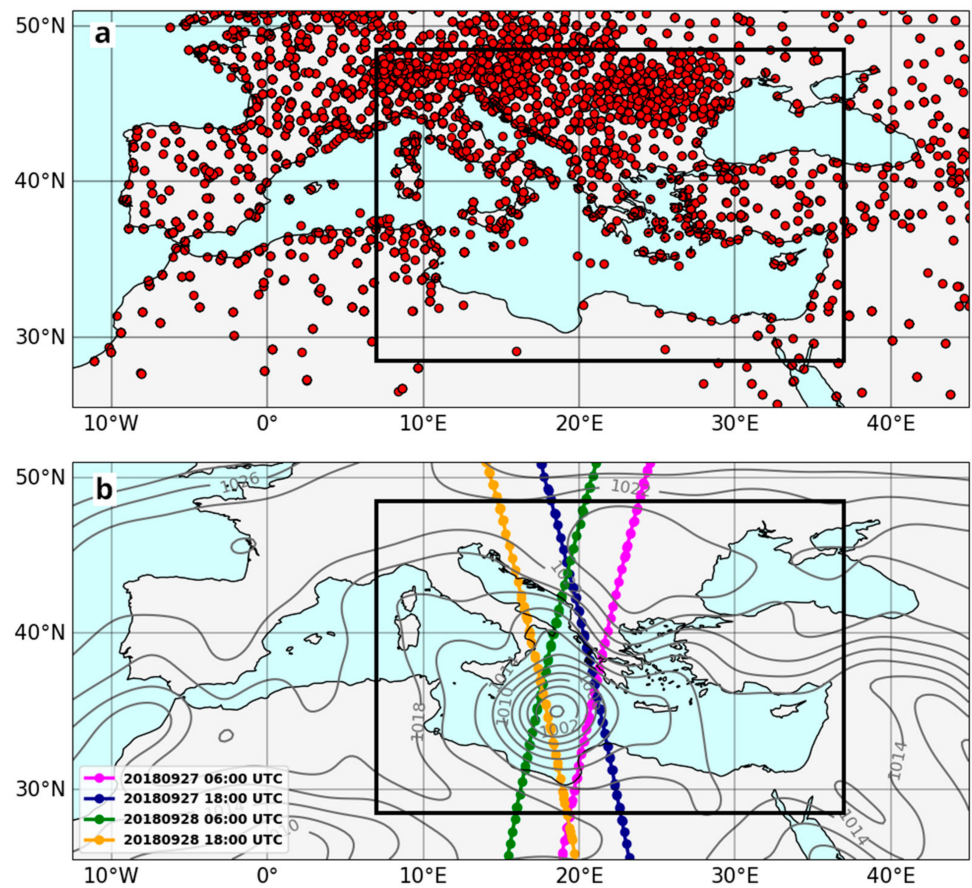


Figure 1. Model coarse domain and fine domain (black line box). (a) Locations (red dots) of conventional data (surface stations) and (b) MSLP from FNL Reanalysis on 28 September 2018, 06:00 UTC (contour lines) and Aeolus tracks (colored dot-lines).

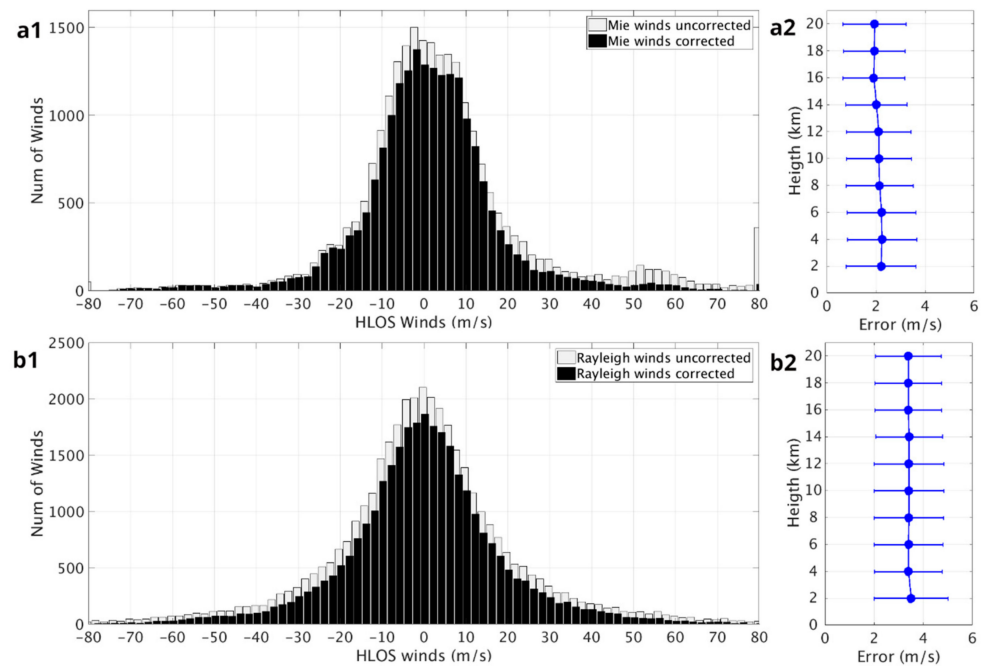


Figure 2. (a1) Corrected and uncorrected Mie-cloud Aeolus L2B winds distribution, (a2) mean instrumental wind speed error and deviation per height for Mie-cloud Aeolus L2B winds, (b1) same as (a1) for Rayleigh-clear Aeolus L2B winds and (b2) same as (a2) for Rayleigh-clear Aeolus L2B winds.

Table 2. Experiment names, data assimilation methods and initialization times.

Experiment Name	Observational Data—Type of Assimilation	Experiment Initialization Times
WRF_Ctrl	None	27 September 2018, 06:00 UTC
WRF_3DVar	Conventional Data—3DVar	27 September 2018, 18:00 UTC
WRF_3DVar_AL2	Conventional Data and Aeolus L2B—3DVar	28 September 2018, 06:00 UTC 28 September 2018, 18:00 UTC

3. Results

During the case study under examination, Aeolus winds were recorded in the broader area where the cyclonic system developed and evolved. Figure 3 depicts the vertical cross sections of HLOS winds stemming from the Mie-cloudy and Rayleigh-clear channels in the north-south range of the WRF coarse domain. The longitude from west to east varies between 25.8° E and 12.9° E. The HLOS winds corresponding to 27 September 2018, 06:00 UTC and 28 September 2018, 06:00 UTC cycles refer to descending orbits, and the other two to ascending, presenting mainly positive wind values. Mie-cloudy winds are concentrated in latitudes approximately in the box 30° N–40° N in accordance with the cyclone spatial extent. Moreover, the detection height is near 10 km, and this might be related to the cloud band tops of medicane Zorbas.

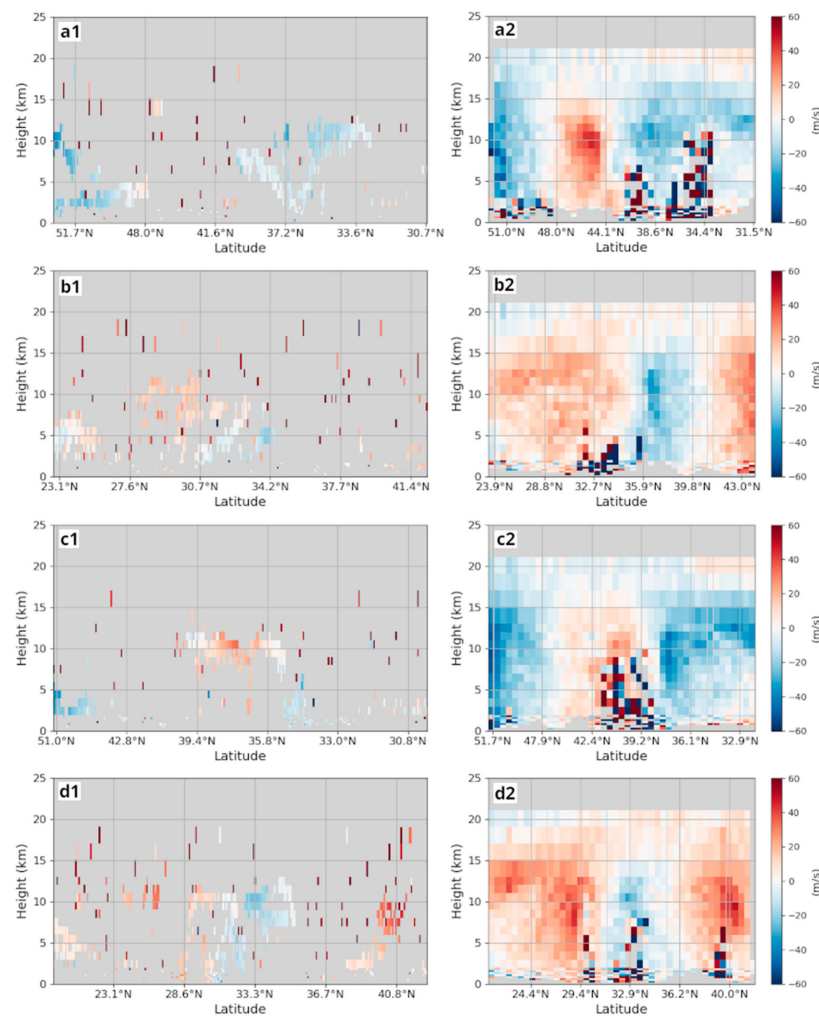


Figure 3. Vertical cross sections of Mie-cloud (left) and Rayleigh-clear (right) Aeolus Level 2B winds within the coarse model domain for (a1,a2) 27 September 2018, 06:00 UTC, (b1,b2) 27 September 2018, 18:00 UTC, (c1,c2) 28 September 2018, 06:00 UTC and (d1,d2) 28 September 2018, 18:00 UTC.

An initial step in assessing the applied data assimilation methodologies was to compare the simulated cyclone tracks for different initialization times (Figure 4). Since all the experiments utilized global forecasting data to update the boundary conditions during runtime, the GFS forecasts were also considered in the analysis. Using the FNL Reanalysis as the best track, all numerical experiments satisfactorily simulated the cyclone path for the first thirty to thirty-six hours of simulation. However, after this period, the modeled tracks generally diverged from the reference track, moving eastward and northeastward across the south Aegean Sea towards Turkey instead of the Greek mainland. This divergence coincided with the approach of the storm to coastal zones and could be attributed to the interaction of the storm with the land, resulting in significant deviations in the simulations.

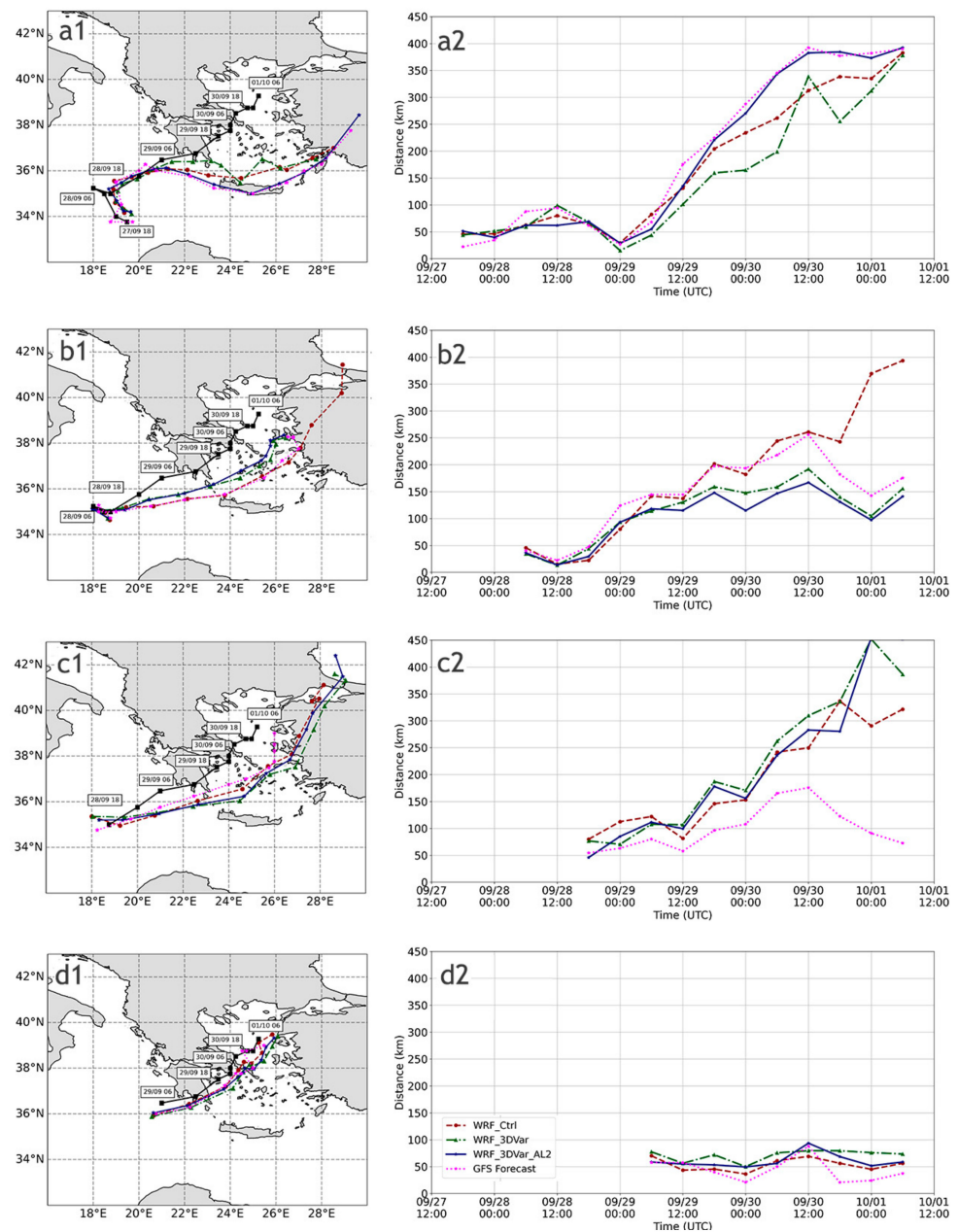


Figure 4. WRF_Ctrl (red line), WRF_3DVar (green line), WRF_3DVar_AL2 (blue line) and GFS (pink line) cyclone tracks (left) and distances (right) from cyclone center of FNL Reanalysis, for simulations initialized on (a1,a2) 27 September 2018, 06:00 UTC, (b1,b2) 27 September 2018, 18:00 UTC, (c1,c2) 28 September 2018, 06:00 UTC and (d1,d2) 28 September 2018, 18:00 UTC.

Among the numerical experiments, those initialized on 28 September 2018, 18:00 UTC performed better overall, indicating increased uncertainty in describing the early stages and the development of the cyclone observed in earlier initialization times. Regarding the impact of data assimilation using conventional observations and conventional observations combined with Aeolus data, as well as the improvement in cyclone tracks compared to the control experiment, the increased variation in the results prevents the drawing of a solid conclusion. Deviations between the results from WRF_Ctrl, WRF_3DVar and WRF_3DVar_AL2 are indeed present and become more visible as the forecasting horizon progresses. An enhancement in cyclone tracking from data assimilation is visible in the model runs initialized on 27 September 2018, 18:00 UTC, while the forecast errors were further reduced with the inclusion of Aeolus winds.

The evolution of the minimum mean sea level pressure (MSLP) values was clearly affected by the initialization time of each experiment as well as the assimilation method followed. In terms of the proper description of the cyclone under study and the tested methods, the simulations initialized on 28 September 2018, 06:00 UTC and 28 September 2018, 18:00 UTC were not as helpful for the analysis, since the event had already evolved. The most important differences in the variation in the minimum MSLP from the different runs were mainly present between the 24 h and 54 h simulation times and reached up to 5 hPa, as shown in the runs initialized on 27 September 2018, 06:00 UTC and 27 September 2018, 18:00 UTC (Figure 5). Divergences after the 54 h simulation time also appear but can be attributed to the different trajectories and locations of the cyclone produced by the methodologies and the interaction with the land. Small differences in the translation speed, close to a 3 h window, are evident among all the simulations in the 27 September 2018, 06:00 UTC experiment and between the WRF_Ctrl and the WRF_3DVar runs with and without the ingestion of Aeolus Lev2B winds in the 27 September 2018, 18:00 UTC experiment. A clear conclusion for the assimilation of the Aeolus winds in the simulation concerning a regular intensification or weakening of the cyclone cannot be achieved. This indicates that each satellite record has a unique influence on the assimilation process. In the 27 September 2018, 06:00 UTC simulation, a temporal shift in the minimum MSLP presents in WRF_3Dvar_AL2, as compared to WRF_3Dvar while in both 27 September 2018, 18:00 UTC and 28 September 2018, 06:00 UTC runs; MSLP values are higher in WRF_3Dvar_AL2 without differences in the variation. Apparently, the impact of Aeolus wind assimilated data has an independent effect in each simulation. When compared with the FNL Reanalysis values that are provided every 6 h, all the experiments show lower MSLP minima, something that can be attributed to the significant differences in the resolution. Nevertheless, there is a general agreement in the evolution. In a qualitative comparison with studies focusing on the same event (e.g., [33]), results partly agree in the temporal variation, in the time framework between 27 September 2018, 12:00 UTC and 29 September 2018, 06:00 UTC, where the cyclone is still in the open sea. Minimum MSLP values, though, are considerably lower, due to the different forcing datasets and methodologies.

To further quantify the impact of the assimilating methodologies, the vertical structure of the cyclone was examined. A vertical cross section of potential vorticity (PV) and wind speed are shown in Figure 6a for the WRF_Ctrl run, during the peak intensity of the cyclone at 29 September 2018, 06:00 UTC. The displayed fields are azimuthally averaged along the axis passing from the cyclone's center. The wind speed reaches its maximum value of over 35 m/s below 1 km above ground level (AGL) close to the center, and the PV reaches 18 PVU in the mid-lower troposphere. In WRF_3DVar (Figure 6b), there are three zones where the PV is clearly reduced: from the surface to less than 1 km AGL and radii less than 50 km from the center of the storm, from 2 to 10 km AGL on the vertical axis and for radii close to 70 km in the same height range as in 2–10 km. There is also a contiguous region where the PV is significantly increased by up to 10 PVU for radii between 30 and 60 km along the vertical axis of rotation. Wind speed is increased by up to 6 m/s in the outer regions of the cyclone and reduced by the same amount in the core of the storm. The WRF_3DVar_AL2 scenario (Figure 6c) shows a similar structure difference

as in WRF_3DVar, although differences from WRF_Ctrl are smaller in general. As indicated by Figure 6d, WRF_3DVar_AL2 produces lower wind speeds at the mid-troposphere and smaller vorticity in the vertical range between 2–8 km, as compared to WRF_3DVar.

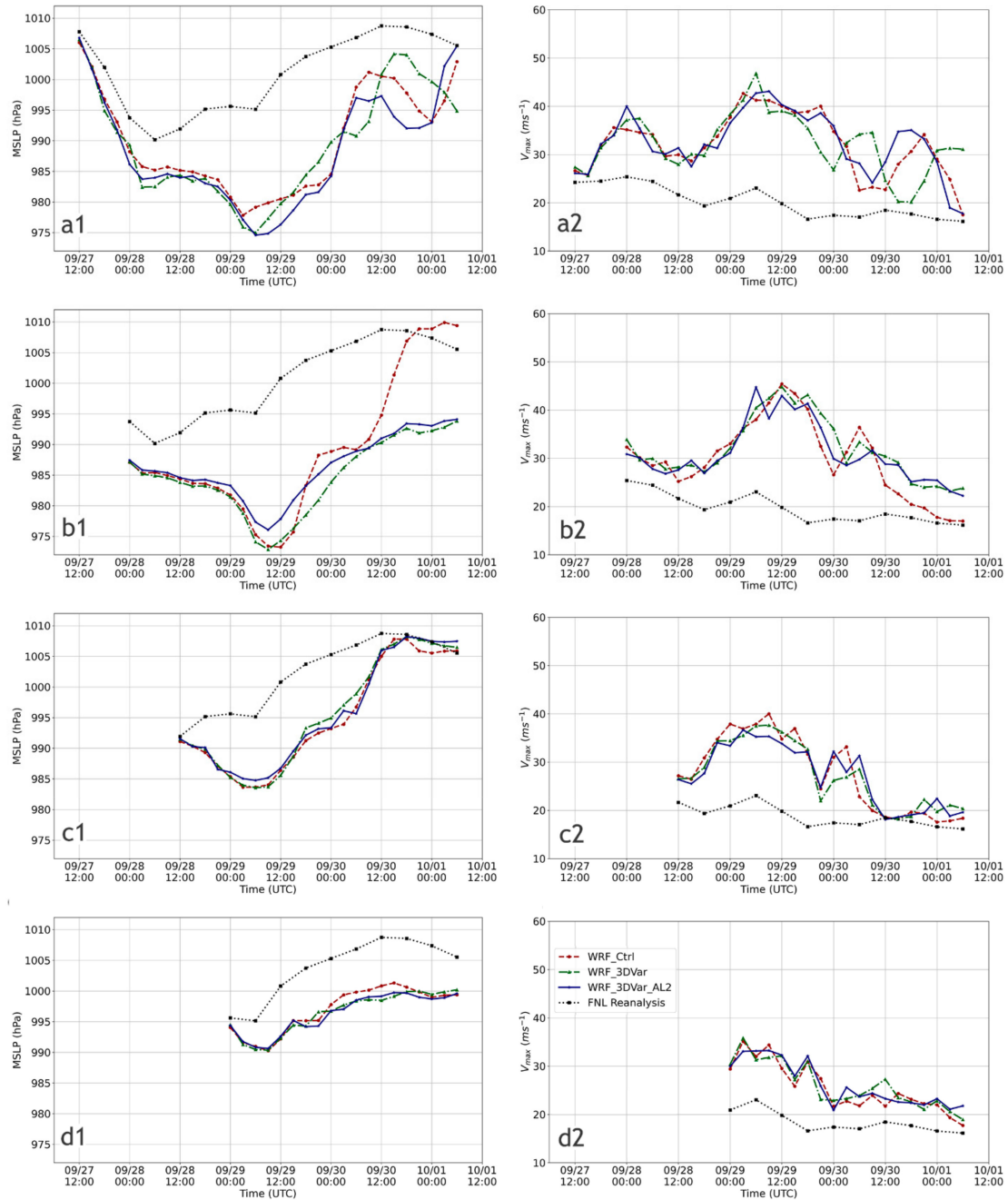


Figure 5. Time series of minimum SLP (left panels) and maximum wind speed at 10 m AGL (right panels) for run cycles (a1,a2) 27 September 2018, 06:00 UTC, (b1,b2) 27 September 2018, 18:00 UTC, (c1,c2) 28 September 2018, 06:00 UTC and (d1,d2) 28 September 2018, 18:00 UTC.

The system is associated with a cut-off low in the middle and upper troposphere (300–500 hPa surface). During the most intense phase of the system, the geopotential height (GPH) at 500 hPa reaches 5540 gpm for the WRF_Ctrl run (Figure 7a). In the WRF_3DVar simulation, the cut-off low is located approximately 100 km northwest with respect to WRF_Ctrl and it is deepened by 60 gpm (Figure 7b). In WRF_3DVar_AL2, the system is also shifted to the northwest, but the geopotential is reduced by only 45 gpm (Figure 7c). A direct comparison between WRF_3DVar and WRF_3DVar_AL2 (Figure 7d) suggests a

displacement of the storm by 100 km in the west-east direction and a greater enhancement for the WRF_3DVar scenario.

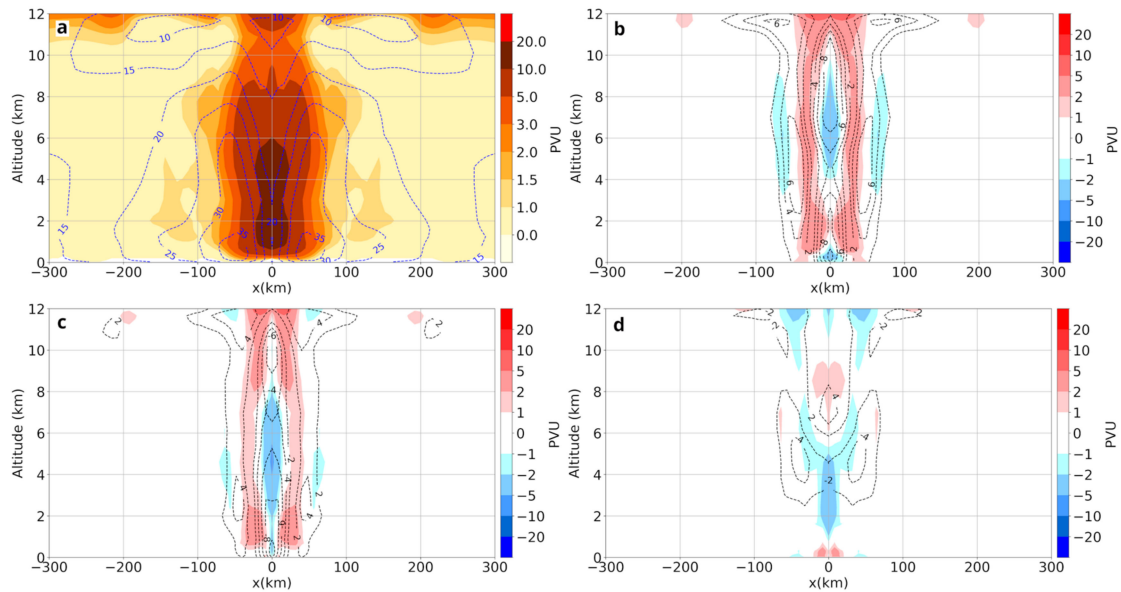


Figure 6. (a) Vertical cross section of PV (brown contours) and wind speed (blue dashed contours) for WRF_Ctrl, (b) differences in PV (colored contours) and wind speed (black dashed contours) for WRF_3DVar minus WRF_Ctrl, (c) same as (b) for WRF_3DVar_AL2 minus WRF_Ctrl and (d) same as (b) for WRF_3DVar_AL2 minus WRF_3DVar. Results refer to azimuthally averaged values around cyclone center for 29 September 2018, 06:00 UTC.

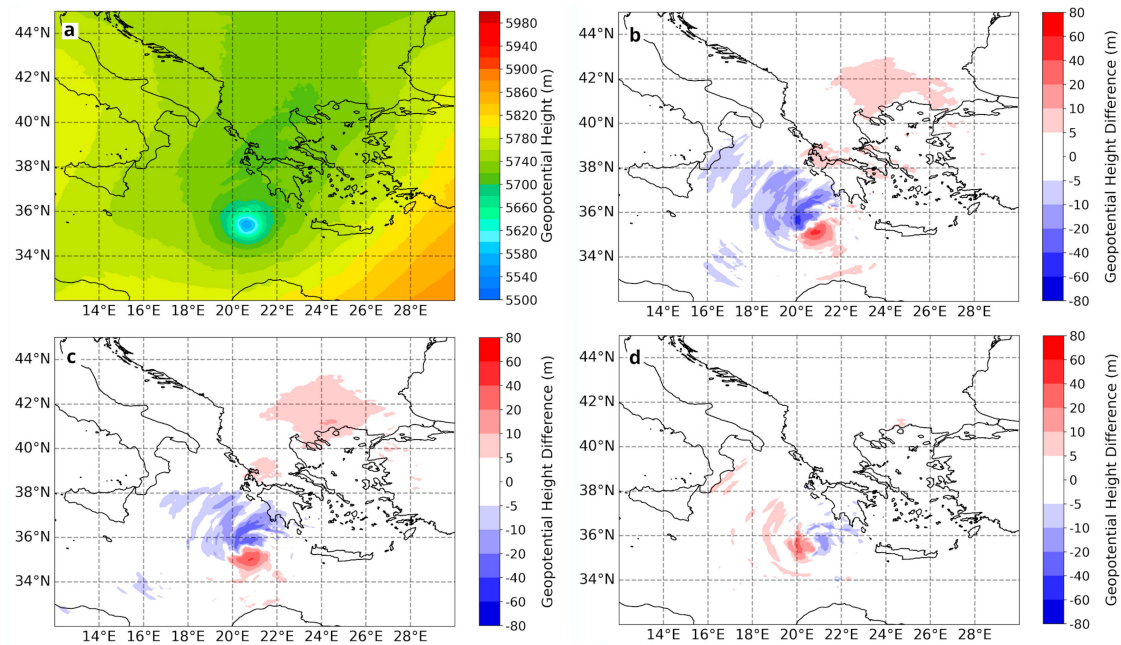


Figure 7. (a) GPH at 500 hPa for WRF_Ctrl, (b) WRF_3DVar minus WRF_Ctrl difference, (c) same as (b) for WRF_3DVar_AL2 minus WRF_Ctrl and (d) same as (b) for WRF_3DVar_AL2 minus WRF_3DVar, for 29 September 2018, 06:00 UTC.

Considering the impacts, the intense rainfall during the event under study caused several issues. Therefore, an additional point for investigation is the effects of the different assimilation methods on precipitation. During a cyclonic event, a potential impact of different initialization data is worth examination not only in terms of accuracy but also in

the spatiotemporal evolution of the rainfall fields. The 24 h accumulated precipitation from the control experiment demonstrates relatively accurate spatial distribution during the two days with the highest precipitation rates as compared with the ones from IMERG data (Figure 8). A decline in performance as the forecast extends to the third day. It is evident that the model does not manage to capture well the significant precipitation that occurred in the mainland.

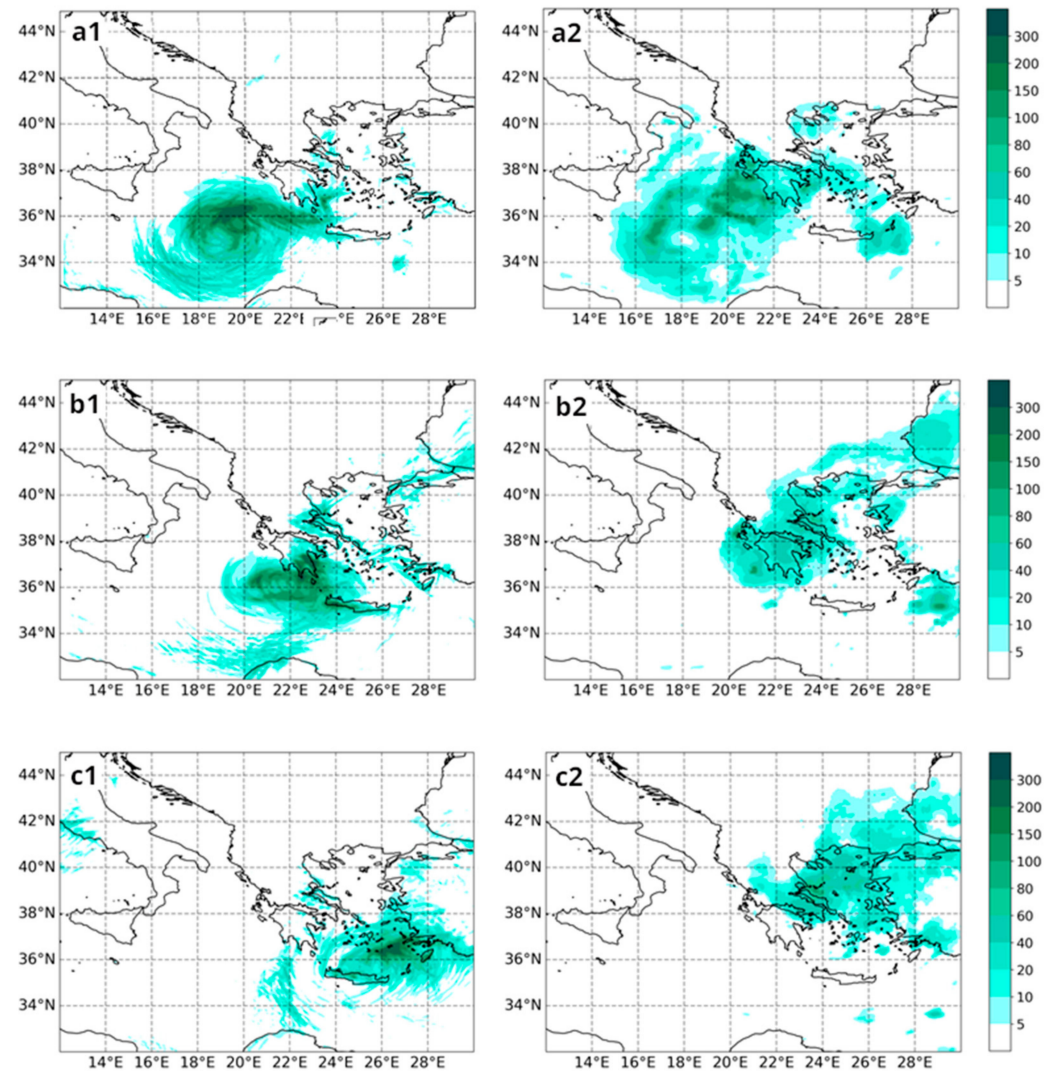


Figure 8. The 24 h accumulated precipitation for WRF_Ctrl (left) and IMERG (right) for (a1,a2) 29 September 2018, 06:00 UTC, (b1,b2) 30 September 2018, 06:00 UTC and (c1,c2) 1 October 2018, 06:00 UTC. Results refer to simulations initiated on 28 September 2018, 06:00 UTC.

To assess the forecasts that utilize assimilation and explore their potential added value, similar fields were created for both sensitivity tests (with and without Aeolus data) (Figure 9). In both scenarios, the observed differences can be attributed to variations associated with the cyclonic development and path. It is evident that even small changes in the track of the cyclone can result in significant variations in the precipitation fields, something also associated with the topography of the region and the local characteristics.

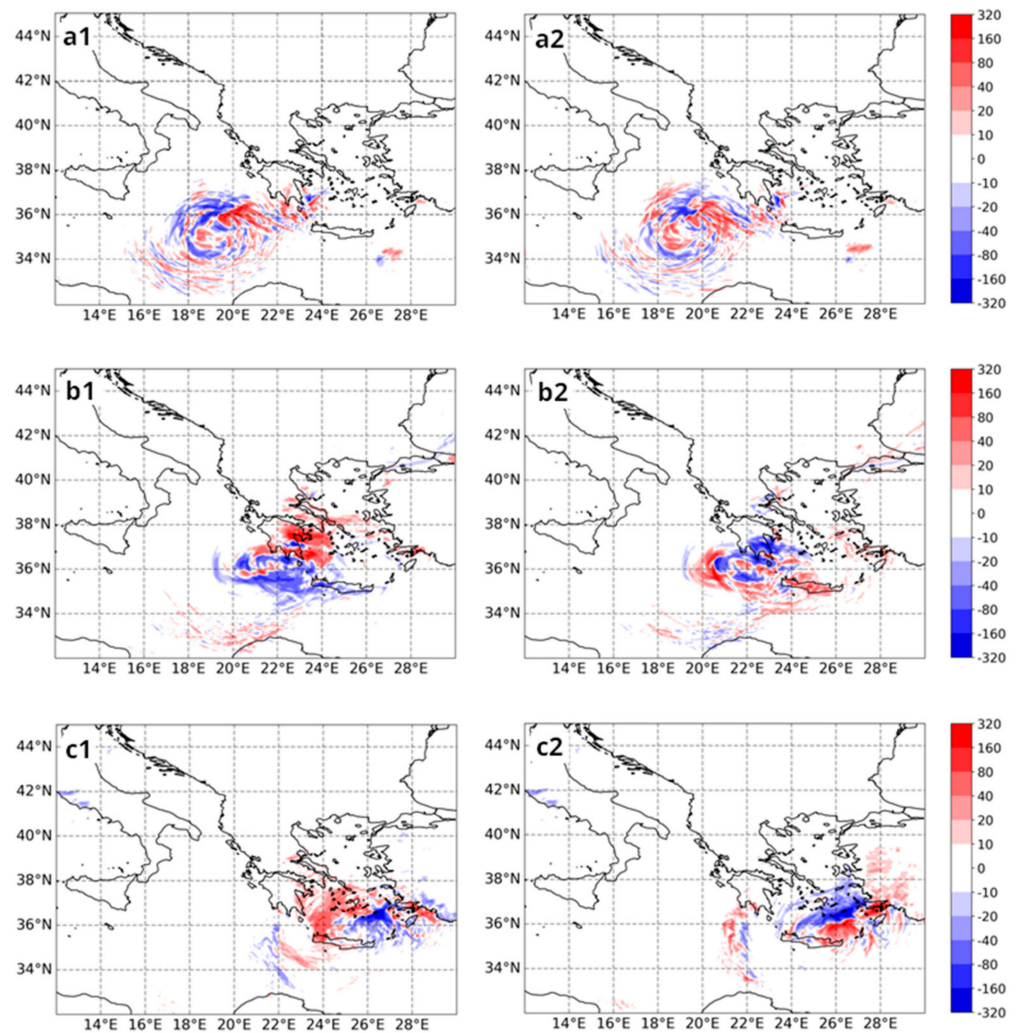


Figure 9. Differences in 24 h accumulated precipitation of WRF_Ctrl minus WRF_3DVar (left) and WRF_3DVar_AL2 minus WRF_Ctrl (right) for (a1,a2) 29 September 2018, 06:00 UTC, (b1,b2) 30 September 2018, 06:00 UTC and (c1,c2) 1 October 2018, 06:00 UTC. Results refer to simulations initiated at 28 September 2018, 06:00 UTC.

During the first forecasting day, both simulations exhibit randomly scattered differences, primarily stemming from minor deviations in the cyclonic track. In the second forecasting horizon, the simulation based on assimilated fields without the influence of Aeolus data shows a clear northward shift in the accumulated precipitation's spatial distribution, as compared to the control simulation. This shift aligns with the IMERG data and corresponds to the observed impacts in the Greek mainland following the event. Conversely, the contribution of Aeolus winds does not yield a clear signal, with most variations appearing random. This pattern continues into the third forecasting horizon. While the distributions do not match the IMERG data, the forecasts based on assimilation fields without Aeolus data tend to place maximum values further in the north.

The spatial differences previously described can be also associated with the differences in the development of the cyclone triggered by the additional ingestion of data during the initialization stage. The total amount of rainfall does not show significant disparities between the several assimilation methods for all undertaken experiments (Figure 10). Differences in the temporal evolution are present as indicated by the smaller or larger deviations and appear in the 6 h hour intervals of rainfall fields.

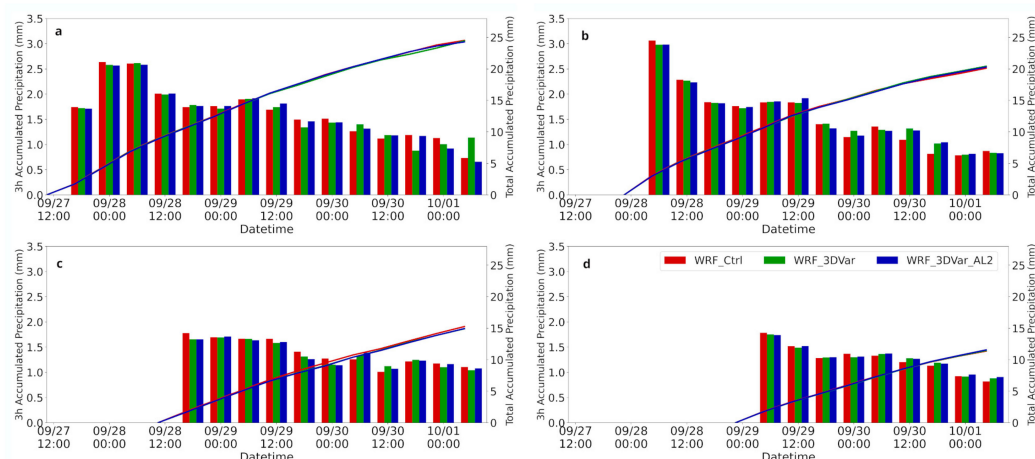


Figure 10. Averaged 6 h accumulated precipitation evolution (bars) and cumulative precipitation (lines) for WRF_Ctrl (red bar and line), WRF_3DVar (green bar and line), WRF_3DVar_AL2 (blue bar and line) runs initialized on (a) 27 September 2018, 06:00 UTC, (b) 27 September 2018, 18:00 UTC, (c) 28 September 2018, 06:00 UTC and (d) 28 September 2018, 18:00 UTC.

4. Discussion and Conclusions

The basis of this study was to investigate the feedback effects stemming from the ingestion of Aeolus wind profiles in a data assimilation system during the development and the evolution of a Mediterranean cyclone. Information on wind profiles is an important aspect of the accuracy of NWP models and, ordinarily, the availability of this type of data is limited. With the aim to incorporate important wind shear atmospheric information, a number of experiments were carried out using the WRF data assimilation model for the ingestion of the Aeolus L2B winds and improvement of the initial state. To investigate the effects of the aforementioned assimilation method, the experiments started at times that coincided with the retrieval of L2B data. In this context, four simulations were performed in sequential mode using a data assimilation process within a 3 h window for enriching the initial state and considering the lifetime of the cyclonic event. The purpose was also to examine the impact and performance in forecasting mode through consecutive runs of different starting dates and times representing independent weather conditions, rather than being restrained in a single experiment that could potentially mislead the conclusions of implementing the Aeolus L2B data in a limited area modeling study. To better assess the effects, simulations with data assimilation of conventional data and without, during the initialization process, were also conducted.

An important process commonly practiced in studies associated with Aeolus products, which was also followed in this work, is the quality control of the data. Mie-cloud and Rayleigh-clear winds were processed for the removal of flagged records and outliers before the ingestion in the WRF data assimilation system. The examination of the results was focused on the basic features of a tropical-like cyclone such as the track, the evolution of minimum MSLP and maximum wind speed values near the center of the cyclone, the upper-air cyclonic structure and the precipitation fields.

Deviations between all the implemented assimilation approaches, smaller or larger, were evident in model results. Variations in minimum MSLP, maximum wind speed and cyclone tracks were mainly present after the 24 h of the simulation, noting the effects triggered from the different assimilating data during the initialization process. However, a solid conclusion for a regular intensification or weakening of the cyclone from the use of Aeolus wind profiles could not be extracted. This indicates that the effects can vary based on the values, the vertical and spatiotemporal coverage and the availability of the Aeolus L2B data. The sensitivity of Aeolus data ingestion in the simulations was also inspected vertically, extended to the middle troposphere. Differences were visible in the upper atmosphere with divergences in PV and GPH. Deviations also emerged in

precipitation, primarily in the spatiotemporal variation of the fields and less in the intensity of the rainfall rates.

The potential use of Aeolus retrievals for forecasting and analysis has been examined and verified in several studies, leading to the incorporation of L2B products in many operational systems. It should be noted, however, that the majority of these studies refer to global-scale systems, having ingested a vast amount of recorded wind profiles and in resolutions similar to the ones of Aeolus data. The current work was focused on the understanding of the effects derived from the assimilation of an innovative satellite product during the development and evolution of a Mediterranean cyclone using a limited area model. The regional scale of this particular study unavoidably results in several constraints. A spatial and temporal alignment between the satellite coverage and such a distinct meteorological event is not frequently attainable. Another limitation for a thorough investigation is the absence of additional types of data, such as that from radiosondes in specific locations coinciding with the model results. Therefore, a rigid outcome for the overall positive feedback of assimilating Aeolus winds in this type of study cannot be obtained. Moreover, different assimilation methodologies, modeling systems and setups could present different responses and performances, specifically in cyclonic events that are characterized by fast-evolving meteorological conditions. Another important factor under consideration in assimilation methodologies is the blending of any ingested data with the initial model conditions derived from the input forcing data, considering the different spatial scales. All points considered, the latest advances in meteorological data acquisition offer new insights into the diagnosis and analysis of weather systems but concurrently render the need for further studies for the proper exploitation of NWP data assimilation techniques. Especially within the context of regional-scale modeling studies and during severe weather events, further investigation is required.

Author Contributions: C.S. performed computations and analysis and wrote the manuscript. I.C. and P.P. aided in analysis, visualization and writing and contributed to the final reading and suggestions. All authors have read and agreed to the published version of the manuscript.

Funding: This research was co-financed by the European Regional Development Fund of the European Union and Greek national funds through the Operational Program Competitiveness, Entrepreneurship and Innovation, under the call Innovation Clusters (project code: IT2CL-0363842).

Institutional Review Board Statement: Not applicable.

Informed Consent Statement: Not applicable.

Data Availability Statement: Data of the Aeolus mission is part of the European Space Agency (ESA) 680 Earth Explorer Programme. This includes the reprocessed L2B wind product accessed via the ESA Aeolus Online Dissemination System from <https://aeolus-ds.eo.esa.int/oads/access/> (accessed on 12 October 2023, European Space Agency). Aeolus L2B data was processed with the VirES visualization tool from <https://aeolus.services/> (accessed on 12 October 2023, EOX IT Service GmbH for European Space Agency). The NCEP operational Global Forecast System analysis and forecasts, Final Reanalysis data and the conventional data were obtained from <https://rda.ucar.edu/datasets/> (accessed on 12 October 2023, National Center for Atmospheric Research). IMERG precipitation data were downloaded from <https://gpm.nasa.gov/data/directory> (accessed on 12 October 2023, Goddard Earth Sciences Data and Information Services Center).

Acknowledgments: Part of this article is based upon work from COST Action CA19109 “MedCyclones”, supported by COST (European Cooperation in Science and Technology). This work was also supported by computational time granted from the National Infrastructures for Research and Technology S.A. (GRNET S.A.) in the National HPC facility—ARIS—under project pr014035_thin-MeDuC.

Conflicts of Interest: The authors declare no conflict of interest.

References

1. Miglietta, M.M. Mediterranean Tropical-Like Cyclones (Medicanes). *Atmosphere* **2019**, *10*, 206. [\[CrossRef\]](#)
2. Flaounas, E.; Davolio, S.; Raveh-Rubin, S.; Pantillon, F.; Miglietta, M.M.; Gaertner, M.A.; Hatzaki, M.; Homar, V.; Khodayar, S.; Korres, G.; et al. Mediterranean cyclones: Current knowledge and open questions on dynamics, prediction, climatology and impacts. *Weather Clim. Dynam.* **2022**, *3*, 173–208. [\[CrossRef\]](#)
3. Hatzaki, M.; Flaounas, E.; Davolio, S.; Pantillon, F.; Patlakas, P.; Raveh-Rubin, S.; Hochman, A.; Kushta, J.; Khodayar, S.; Dafis, S.; et al. MedCyclones: Working Together toward Understanding Mediterranean Cyclones. *Bull. Am. Meteorol. Soc.* **2023**, *104*, E480–E487. [\[CrossRef\]](#)
4. Flaounas, E.; Aragão, L.; Bernini, L.; Dafis, S.; Doiteau, B.; Flocas, H.; Gray, S.L.; Karwat, A.; Kouroutzoglou, J.; Lionello, P.; et al. A composite approach to produce reference datasets for extratropical cyclone tracks: Application to Mediterranean cyclones. *Weather Clim. Dynam.* **2023**, *4*, 639–661. [\[CrossRef\]](#)
5. Patlakas, P.; Stathopoulos, C.; Tsalis, C.; Kallos, G. Wind and wave extremes associated with tropical-like cyclones in the Mediterranean basin. *Int. J. Climatol.* **2021**, *41*, E1623–E1644. [\[CrossRef\]](#)
6. Patlakas, P.; Chaniotis, I.; Hatzaki, M.; Kouroutzoglou, J.; Flocas, H.A. The eastern Mediterranean extreme snowfall of January 2022: Synoptic analysis and impact of sea-surface temperature. *Weather* **2023**, *early version*. [\[CrossRef\]](#)
7. Panegrossi, G.; D’Adderio, L.P.; Dafis, S.; Rysman, J.-F.; Casella, D.; Dietrich, S.; Sanò, P. Warm Core and Deep Convection in Medicanes: A Passive Microwave-Based Investigation. *Remote Sens.* **2023**, *15*, 2838. [\[CrossRef\]](#)
8. Ferrarin, C.; Pantillon, F.; Davolio, S.; Bajo, M.; Miglietta, M.M.; Avolio, E.; Carrió, D.S.; Pytharoulis, I.; Sanchez, C.; Patlakas, P.; et al. Assessing the coastal hazard of Mediane Ianos through ensemble modelling. *Nat. Hazards Earth Syst. Sci.* **2023**, *23*, 2273–2287. [\[CrossRef\]](#)
9. Wang, C.; Wilson, D.; Haack, T.; Clark, P.; Lean, H.; Marshall, R. Effects of Initial and Boundary Conditions of Mesoscale Models on Simulated Atmospheric Refractivity. *J. Appl. Meteorol. Climatol.* **2012**, *51*, 115–132. [\[CrossRef\]](#)
10. Ferrari, F.; Cassola, F.; Tjuu, P.E.; Stocchino, A.; Broto, P.; Mazzino, A. Impact of Model Resolution and Initial/Boundary Conditions in Forecasting Flood-Causing Precipitations. *Atmosphere* **2020**, *11*, 592. [\[CrossRef\]](#)
11. Barker, D.; Huang, X.-Y.; Liu, Z.; Auligné, T.; Zhang, X.; Rugg, S.; Ajjaji, R.; Bourgeois, A.; Bray, J.; Chen, Y.; et al. The Weather Research and Forecasting Model’s Community Variational/Ensemble Data Assimilation System: WRFDA. *Bull. Am. Meteorol. Soc.* **2012**, *93*, 831–843. [\[CrossRef\]](#)
12. Tan, P.-H.; Soong, W.-K.; Tsao, S.-J.; Chen, W.-J.; Chen, I.-H. Impact of Lidar Data Assimilation on Simulating Afternoon Thunderstorms near Pingtung Airport, Taiwan: A Case Study. *Atmosphere* **2022**, *13*, 1341. [\[CrossRef\]](#)
13. Samos, I.; Flocas, H.; Louka, P. A Background Error Statistics Analysis over the Mediterranean: The Impact on 3DVAR Data Assimilation. *Environ. Sci. Proc.* **2023**, *26*, 158.
14. Shahzad, R.; Shah, M.; Ahmed, A. Comparison of VTEC from GPS and IRI-2007, IRI-2012 and IRI-2016 over Sukkur Pakistan. *Astrophys. Space Sci.* **2021**, *366*, 42. [\[CrossRef\]](#)
15. Baker, W.E.; Atlas, R.; Cardinali, C.; Clement, A.; Emmitt, G.D.; Gentry, B.M.; Hardesty, R.M.; Källén, E.; Kavaya, M.J.; Langland, R.; et al. Lidar-Measured Wind Profiles: The Missing Link in the Global Observing System. *Bull. Am. Meteorol. Soc.* **2014**, *95*, 543–564. [\[CrossRef\]](#)
16. Reitebuch, O.; Lemmerz, C.; Nagel, E.; Paffrath, U.; Durand, Y.; Endemann, M.; Fabre, F.; Chaloupy, M. The Airborne Demonstrator for the Direct-Detection Doppler Wind Lidar ALADIN on ADM-Aeolus. Part I: Instrument Design and Comparison to Satellite Instrument. *J. Atmos. Ocean. Technol.* **2009**, *26*, 2501–2515. [\[CrossRef\]](#)
17. Laroche, S.; St-James, J. Impact of the Aeolus Level-2B horizontal line-of-sight winds in the Environment and Climate Change Canada global forecast system. *Q. J. R. Meteorol. Soc.* **2022**, *148*, 2047–2062. [\[CrossRef\]](#)
18. Martin, A.; Weissmann, M.; Cress, A. Investigation of links between dynamical scenarios and particularly high impact of Aeolus on numerical weather prediction (NWP) forecasts. *Weather Clim. Dynam.* **2023**, *4*, 249–264. [\[CrossRef\]](#)
19. Garrett, K.; Liu, H.; Ide, K.; Hoffman, R.N.; Lukens, K.E. Optimization and impact assessment of Aeolus HLOS wind assimilation in NOAA’s global forecast system. *Q. J. R. Meteorol. Soc.* **2022**, *148*, 2703–2716. [\[CrossRef\]](#)
20. Rennie, M.P.; Isaksen, L.; Weiler, F.; de Kloe, J.; Kanitz, T.; Reitebuch, O. The impact of Aeolus wind retrievals on ECMWF global weather forecasts. *Q. J. R. Meteorol. Soc.* **2021**, *147*, 3555–3586. [\[CrossRef\]](#)
21. Rani, S.I.; Jangid, B.P.; Kumar, S.; Bushair, M.T.; Sharma, P.; George, J.P.; George, G.; Das Gupta, M. Assessing the quality of novel Aeolus winds for NWP applications at NCMRWF. *Q. J. R. Meteorol. Soc.* **2022**, *148*, 1344–1367. [\[CrossRef\]](#)
22. Feng, C.; Pu, Z. The impacts of assimilating Aeolus horizontal line-of-sight winds on numerical predictions of Hurricane Ida (2021) and a mesoscale convective system over the Atlantic Ocean. *Atmos. Meas. Tech.* **2023**, *16*, 2691–2708. [\[CrossRef\]](#)
23. Hagelin, S.; Azad, R.; Lindskog, M.; Schyberg, H.; Körnich, H. Evaluating the use of Aeolus satellite observations in the regional numerical weather prediction (NWP) model Harmonie–Arome. *Atmos. Meas. Tech.* **2021**, *14*, 5925–5938. [\[CrossRef\]](#)
24. Matsangouras, I.; Avgoustoglou, E.; Pytharoulis, I.; Nastos, P. The Impact of Aeolus Wind Profile Measurements on Severe Weather Events: A COSMO NWP Case Study over Thessaly. *Environ. Sci. Proc.* **2023**, *26*, 47.
25. Kiriakidis, P.; Gkikas, A.; Papangelis, G.; Christoudias, T.; Kushta, J.; Proestakis, E.; Kampouri, A.; Marinou, E.; Drakaki, E.; Benedetti, A.; et al. The impact of assimilating Aeolus wind data on regional Aeolian dust model simulations using WRF-Chem. *EGU sphere* **2022**, *2022*, 1–42. [\[CrossRef\]](#)

26. Skamarock, W.C.; Klemp, J.B.; Dudhia, J.; Gill, D.O.; Liu, Z.; Berner, J.; Wang, W.; Powers, J.G.; Duda, M.G.; Barker, D.; et al. *A Description of the Advanced Research WRF Model Version 4*; NCAR Technical Notes NCAR/TN-556+STR; National Center for Atmospheric Research: Boulder, CO, USA, 2019; p. 145. [[CrossRef](#)]
27. Patlakas, P.; Stathopoulos, C.; Kalogeri, C.; Vervatis, V.; Karagiorgos, J.; Chaniotis, I.; Kallos, A.; Ghulam, A.S.; Al-omary, M.A.; Papageorgiou, I.; et al. The development and operational use of an integrated Numerical Weather Prediction System in the National Center of Meteorology of the Kingdom of Saudi Arabia. *Weather Forecast.* **2023**, *38*, 2289–2319. [[CrossRef](#)]
28. Wang, X.; Barker, D.M.; Snyder, C.; Hamill, T.M. A Hybrid ETKF–3DVAR Data Assimilation Scheme for the WRF Model. Part II: Real Observation Experiments. *Mon. Weather Rev.* **2008**, *136*, 5132–5147. [[CrossRef](#)]
29. Thodsan, T.; Wu, F.; Torsri, K.; Cuestas, E.M.A.; Yang, G. Satellite Radiance Data Assimilation Using the WRF-3DVAR System for Tropical Storm Dianmu (2021) Forecasts. *Atmosphere* **2022**, *13*, 956. [[CrossRef](#)]
30. ESA. *ESA SP-1311 ADM-Aeolus Science Report*; European Space Agency (ESA): Paris, France, 2008; 121p, ISBN 978-92-9221-404-3.
31. Rennie, M.P.; Isaksen, L. *The NWP Impact of Aeolus Level-2B Winds at ECMWF*; Technical Memo 864; ECMWF: Reading, UK, 2020. [[CrossRef](#)]
32. Portmann, R.; González-Alemán, J.; Sprenger, M.; Wernli, H. Medicane Zorbas: Origin and effects of an uncertain upper-level PV streamer. In *Geophysical Research Abstracts*; Copernicus Gesellschaft mbH: Göttingen, Germany, 2019; p. 2425.
33. Stathopoulos, C.; Patlakas, P.; Tsalis, C.; Kallos, G. The Role of Sea Surface Temperature Forcing in the Life-Cycle of Mediterranean Cyclones. *Remote Sens.* **2020**, *12*, 825. [[CrossRef](#)]
34. Varlas, G.; Vervatis, V.; Spyrou, C.; Papadopoulou, E.; Papadopoulos, A.; Katsafados, P. Investigating the impact of atmosphere–wave–ocean interactions on a Mediterranean tropical-like cyclone. *Ocean Model.* **2020**, *153*, 101675. [[CrossRef](#)]
35. Jiménez, P.A.; Dudhia, J.; González-Rouco, J.F.; Navarro, J.; Montávez, J.P.; García-Bustamante, E. A Revised Scheme for the WRF Surface Layer Formulation. *Mon. Weather Rev.* **2012**, *140*, 898–918. [[CrossRef](#)]
36. Niu, G.-Y.; Yang, Z.-L.; Mitchell, K.E.; Chen, F.; Ek, M.B.; Barlage, M.; Kumar, A.; Manning, K.; Niyogi, D.; Rosero, E.; et al. The community Noah land surface model with multiparameterization options (Noah-MP): 1. Model description and evaluation with local-scale measurements. *J. Geophys. Res. Atmos.* **2011**, *116*, D12. [[CrossRef](#)]
37. Hong, S.-Y.; Noh, Y.; Dudhia, J. A New Vertical Diffusion Package with an Explicit Treatment of Entrainment Processes. *Mon. Weather Rev.* **2006**, *134*, 2318–2341. [[CrossRef](#)]
38. Mlawer, E.J.; Taubman, S.J.; Brown, P.D.; Iacono, M.J.; Clough, S.A. Radiative transfer for inhomogeneous atmospheres: RRTM, a validated correlated-k model for the longwave. *J. Geophys. Res. Atmos.* **1997**, *102*, 16663–16682. [[CrossRef](#)]
39. Kain, J.S. The Kain–Fritsch Convective Parameterization: An Update. *J. Appl. Meteorol.* **2004**, *43*, 170–181. [[CrossRef](#)]
40. Parrish, D.F.; Derber, J.C. The National Meteorological Center’s Spectral Statistical-Interpolation Analysis System. *Mon. Weather Rev.* **1992**, *120*, 1747–1763. [[CrossRef](#)]

Disclaimer/Publisher’s Note: The statements, opinions and data contained in all publications are solely those of the individual author(s) and contributor(s) and not of MDPI and/or the editor(s). MDPI and/or the editor(s) disclaim responsibility for any injury to people or property resulting from any ideas, methods, instructions or products referred to in the content.